Ann. Occup. Hyg., 2014, Vol. 58, No. 9, 1175–1185
doi:10.1093/annhyg/meu051
Advance Access publication 3 September 2014

BOHS The Chartered Society for Worker Health Protection

Simulated Effects of Head Movement on Contact Pressures Between Headforms and N95 Filtering Facepiece Respirators-Part 1: Headform Model and Validation

Zhipeng Lei[1], Xuewu Ji[2], Ning Li[1], James Yang[1,*], Ziqing Zhuang[3] and Dana Rottach[3]

1.Department of Mechanical Engineering, Human-Centric Design Research Laboratory, Texas Tech University, Lubbock, TX 79409, USA
2.State Key Lab of Automotive Safety and Energy, Tsinghua University, Beijing 100084, China
3.National Institute for Occupational Safety and Health, Pittsburgh, PA 15236, USA
*Author to whom correspondence should be addressed. Tel: +1-806-834-6746; fax: +1-806-742-3540; e-mail: james.yang@ttu.edu
Submitted 19 October 2013; revised 4 June 2014; revised version accepted 17 June 2014.

ABSTRACT

In a respirator fit test, a subject is required to perform a series of exercises that include moving the head up and down and rotating the head left and right. These head movements could affect respirator sealing properties during the fit test and consequently affect fit factors. In a model-based system, it is desirable to have similar capability to predict newly designed respirators. In our previous work, finite element modeling (FEM)-based contact simulation between a headform and a filtering facepiece respirator was carried out. However, the headform was assumed to be static or fixed. This paper presents the first part of a series study on the effect of headform movement on contact pressures—a new headform with the capability to move down (flexion), up (extension), and rotate left and right-and validation. The newly developed headforms were validated for movement by comparing the simulated cervical vertebrae rotation angles with experimental results from the literature.

KEYWORDS: contact pressure; finite element method; filtering facepiece respirator; headform; head movement

INTRODUCTION

Head movements affect respirator fit (Lee *et al.*, 2005; Grinshpun *et al.*, 2009) due to the relative position change between a respirator and a human face, potentially causing faceseal leaks (Crutchfield *et al.*, 1999). The Occupational Safety and Health Administration (OSHA) respiratory protection regulation defines a standard eight-exercise procedure in most respirator fit tests. During these respirator fit tests, the exercises, specifically (i) normal breathing without talking; (ii) deep breathing; (iii) moving the head side to side; (iv) moving the head up and down; (v) talking; (vi) grimacing by smiling or frowning; (vii) bending at the waist; and (viii) normal breathing, are performed in sequence (OSHA, 1999). This study focused on the effect of moving the head side to side and turning the

head up and down on the contact between a respirator and a head.

Finite element modeling (FEM) has been used for studying interactions between headforms and respirators (Bitterman, 1991; Piccione *et al.*, 1997; Yang *et al.*, 2009; Dai *et al.*, 2011). However, the headform model was either a rigid or deformable single shell, lacking biofidelity, and the respirator model was modeled by a single layer of facepiece, and lacked straps and the nose clip. Advanced 3D finite element (FE) models of faces were developed with complicated structures, including bones, fat, muscle, and skin, according to human facial anatomy (Chabanas *et al.*, 2003; Barbarino *et al.*, 2009). Using the advanced face models, soft tissue deformation was simulated either by displacing the bones or by imposing gravity loads. In another advanced 3D FE face model created by Beldie *et al.* (2010), facial expressions were simulated by contracting the facial muscles. Lei *et al.* (2012) reported an advanced model for investigating the interaction between a respirator and headform. However, headform movement was not considered in these simulations.

To study the effects of head movement, it is important to have a new headform model that can mimic human head movement. An understanding of the anatomy of the head and neck is critical to the development of this new headform model. Seven cervical vertebrae C1–C7 control the head movements of extension, flexion, and rotation (Drake *et al.*, 2005). FEM has been commonly used for studying behaviors of cervical spines under external loads (Goel and Clausen, 1998; Yoganandan *et al.*, 2001; Ng *et al.*, 2004; Zhang *et al.*, 2006, 2008; del Palomar *et al.*, 2008). A biomechanical model of a cervical spine typically includes cervical vertebrae, ligaments, intervertebral discs, facet joints, and muscles. The cervical spine model can be connected to a head model for controlling the head movements. Different kinds of head movements, including flexion, extension, axial rotation, and bending, were simulated by applying external loads to the FE cervical spine model (Van der Horst, 2002; Esat *et al.*, 2005; Hedenstierna and Halldin, 2008; Esat and Acar, 2009; Hedenstierna *et al.*, 2009). The above existing head models do not include any skin or fatty tissue. For contact between a respirator and a headform, the skin and fatty tissue, as well as respirator facepiece, have deformation. Therefore, previous rigid or single shell headform models with a cervical spine model are not adequate for the purpose of this study.

The ultimate goal of this study is to develop computer-based methods to simulate all of the exercises performed in the respirator fit test. The objective of this work is to develop new headform models that can simulate head movement. We describe here a new cervical spine model, assembly of deformable and multilayer headforms with the cervical spine model to form new headform models, and validation of the new headform models. In a separate paper (Lei *et al.*, 2014), we will implement these newly developed headform models to study the effects of head movement on contact pressures between headforms and respirators.

NEW HEADFORM MODELS

In order to have the ability to rotate, new headforms were developed that included the existing National Institute for Occupational Safety and Health (NIOSH) headforms (Zhuang *et al.*, 2010; Lei *et al.*, 2012) and the cervical spine model. To build the new headform, a cervical spine model including cervical vertebrae, intervertebral discs, ligaments, and facet joints was generated. Layers of skin, muscle, fatty tissue, and bone were then added to the headform model (Lei *et al.*, 2012). The cervical spine model and the headform model were then assembled to form the new FE headforms. Finally, the head movements of the new headform were defined.

The main components of the cervical spine model were the cervical vertebrae C1–C7 (see Fig. 1), which were modeled as rigid triangular surfaces and were determined from the openly accessible BodyParts3D database (Mitsuhashi *et al.*, 2009). The BodyParts3D database provides geometrical surfaces of body components in a whole-body model of an adult human male. The cervical spine model used the cervical vertebrae C1–C7 in the whole-body model. Each vertebra from C3 to C7 was modeled as a vertebra body and a posterior vertebral arch. C1 had an arch and a posterior vertebral arch, and C2 had a dens (odontoid process) and a posterior vertebral arch. Initial relative positions of C1–C7 (lordotic curve) in our cervical spine model were maintained the same as those in the BodyParts3D whole-body model.

Five intervertebral discs were placed to separate the vertebrae C2–C7. In studies of head impact simulations, the intervertebral discs have been modeled

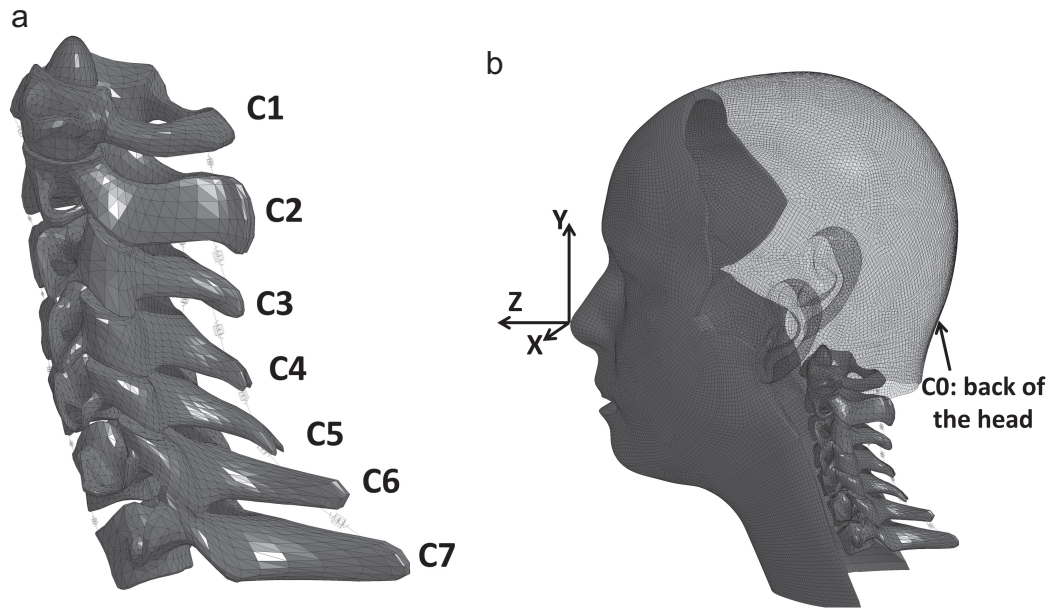

1 (a) The cervical spine model; (b) The new FE headform model with the global coordinate system.

as deformable FE bodies to calculate stresses and deformations of the intervertebral discs for injury evaluation (Goel and Clausen, 1998; Ng *et al.*, 2004; Zhang *et al.*, 2006, 2008; del Palomar *et al.*, 2008). In the field of respirator study, the stresses and deformations of the intervertebral discs are not of concern. The intervertebral discs were therefore simplified to spherical joints. Each spherical joint was located at the center of the gap between two vertebral bodies of C2–C3 to C6–C7. The spherical joint for connecting C1 and C2 was defined as the contact point between the arc of C1 and the dens of C2. The back of the head (rigid), referred as C0, was combined with C1 by a spherical joint. C1's two facets create a pair of condyloid joints that articulate C1 and the occipital bone. The pair of condyloid joints was simplified as a C0–C1 spherical joint. The C0–C1 spherical joint was defined at the middle point of the line connecting the centers of two facet surfaces of C1.

Panjabi *et al.* (2001) and Wheeldon *et al.* (2006) provided experimental results of rotations between two adjacent cervical vertebrae (C1–C2 to C6–C7) due to flexion, extension, and rotation. The load-displacement curves obtained in the experimental measurements were all nonlinear. In this paper, we assumed that the intervertebral discs and the ligaments equally contributed to the stiffness of the rotation between two cervical vertebrae, following the approach proposed by Van der Horst (2002). The flexion/extension stiffness of the spherical joint was defined as half of the flexion/extension stiffness functions of C1–C2 to C6–C7 measured by Wheeldon *et al.* (2006) and Panjabi *et al.* (2001), and the rotation stiffness of the spherical joints was defined as half of the (left/right) rotation stiffness functions of C1–C2 to C6–C7 measured by Panjabi *et al.* (2001). Viscoelastic behaviors of the spherical joints were considered by introducing damping forces to the spherical joints using damping coefficients from Van der Horst (2002).

Ligaments in the cervical spine model connected adjacent cervical vertebrae and were modeled as discrete elements defined as lines between nodes on the cervical vertebrae. Facet joints in the cervical spine model linked the articular surfaces of pairs of adjacent cervical vertebrae (C2–C3 to C6–C7) and were modeled as discrete elements. Locations of the ligaments and the facet joints in the cervical spine model were taken from the literature (Yoganandan *et al.*, 2001; Zhang *et al.*, 2006, 2008; del Palomar *et al.*, 2008). Ligaments and facet joints were modeled using the viscoelastic Kelvin–Voigt model, consisting of a spring and damper pair connected in parallel. Mechanical properties of the ligaments and the facet joints were based on experimental studies (Yoganandan *et al.*,

2001). Because movements of the cervical spine model were driven by external moments in simulations, the cervical spine model did not include active muscles. Passive muscles in the neck region, modeled as a thick layer, were considered as a component in the headform instead of that in the cervical spine model. Table 1 summarizes the mechanical properties of the components in the cervical spine model.

Five FE headforms from NIOSH's digital headform models previously developed by Lei *et al.* (2012) include segments of the forehead, left cheek, right cheek, chin, neck, and the back of the head. The facial regions have multilayer structures including skin, muscle, fatty tissue, and bone, head movement is not considered, and the isotropic Hooke's law (elastic model) is used to define the mechanical properties of the skin, muscle, and fatty tissue.

When head movements are considered, strains of the skin, muscle, and fatty tissue would reach values of 20%, and hyperelastic laws should be used to obtain more realistic strain–stress relationship (Delalleau *et al.*, 2008). Multilayer headform models were developed, having the same segments and structures as the previously developed FE headforms, and using hyperelastic models to define the mechanical properties of the skin, muscle, and fatty tissue. The bones and the back of the head were simplified as rigid models. The mechanical properties of the headform layers are shown in Table 2.

The new headforms were formed by assembling the cervical spine model with the multilayer headform models. The cervical spine model and one of the multilayer headform models were imported into the same virtual environment in LS-PrePost software (Livermore Software Technology Corporation, Livermore, CA, USA). The two models were positioned based on the same coordinate system. A global coordinate system was defined where the *z*-axis is normal to the headform frontal face, the *x*-axis is along the lateral direction of the headform towards the headform frontal face's left, and the *y*-axis is defined by the right-hand rule in Fig. 1b. The origin of the global coordinate system was located at the point of the nasal tip. The new headform models had different types of elements shown in Table 3. All five newly developed headforms had the same cervical spine model but with different headform models from NIOSH.

The total head movements (extension, flexion, left rotation, and right rotation) were defined as the rotation angles with respect to the global axes. This study did not consider lateral bending because the respirator fit test does not require lateral bending movement (OSHA, 1999; Viscusi *et al.*, 2011). The total head

Table 1. Stiffness and damping values for intervertebral discs, ligaments, and facet joints in the cervical spine model

Tissue		Stiffness	Damping	Source
Joints for the intervertebral discs and the den-arc	Flexion	Nonlinear	1.5 Nms rad^{-1}	Wheeldon *et al.* (2006) and van der Horst (2002)
	Extension	Nonlinear	1.5 Nms rad^{-1}	
	Rotation	Nonlinear	1.5 Nms rad^{-1}	Panjabi *et al.* (2001) and van der Horst (2002)
Ligaments	ALL	16 N mm^{-1}	4e-4 Ns mm^{-1}	Yoganandan *et al.* (2001)
	PLL	25 N mm^{-1}	4e-4 Ns mm^{-1}	
	CL	19 N mm^{-1}	4e-4 Ns mm^{-1}	
	ISL	7 N mm^{-1}	4e-4 Ns mm^{-1}	
	AM	24 N mm^{-1}	4e-4 Ns mm^{-1}	
	LF	25 N mm^{-1}	4e-4 Ns mm^{-1}	
Facet joints	JC	32 N mm^{-1}	4e-4 Ns mm^{-1}	

AM, anterior membrane; ALL, anterior longitudinal ligament; CL, cervical ligament; FL, flaval ligament; ISL, interspinous ligament; JC, joint capsules; LF, ligamentum flavum; PLL, posterior longitudinal ligament.

Table 2. Mechanical properties of headform layers

Layer	Skin	Muscle	Fatty tissue	Bone	Back of head
Material	Hyperelastic	Ogden hyperelastic	Ogden hyperelastic	Rigid	Rigid
Density (Kg m^{-3})	920	920	920	4500	4500
Poisson ratio	0.499	0.499	0.499	0.30	0.30
Stiffness parameters	C_{10} = 0.0094 MPa	μ_i = 0.013337	$\mu_i = 3 \times 10^{-5}$	E = 100	E = 100
	C_{10} = 0.0082 MPa	α_i = 14.5	α_i = 20	MPa	MPa
		G_i = 0.522,0.211, 0.375, 0.290, 0.80	$G_i = 3 \times 10^{-3}$		
		β_i = 1020, 400, 65, 30, 0.1	β_i = 310		
Source	Hendriks *et al.* (2003)	Hedenstierna and Halldin (2008)	Engelbrektsson (2011)		

Table 3. Elements of new headforms

Headform	Solid elements	Shell elements	Discrete elements
Large	71 440	59 005	68
Medium	56 937	54 084	68
Small	40 400	51 370	68
Long/narrow	56 197	57 520	68
Short/wide	53 942	53 791	68

movements were the summation of seven relative movements of C0–C1 to C6–C7. Seven local coordinate systems of C0–C1 to C6–C7 were defined for the relative movements of C0–C1 to C6–C7. Each local coordinate origin of C2–C3 to C6–C7 was at the center of the gap between two vertebral bodies. The local coordinate origin of C0–C1 was the intersection of the sagittal plane of the extended headform and the line connecting the centers of two facet surfaces of C1. The local coordinate origin of C1–C2 was the contact point between the arc and den. The $X_{i\,i+1-}$, $Y_{i\,i+1-}$, and $Z_{i\,i+1-}$ axes of the local coordinate systems of C*i*–C*i* + *1* (i = 0, 1, 2, … , 5) were parallel to the X-, Y-, and Z-axes of the global coordinate system. Being fixed at C*i* + *1*, the local coordinate system of C*i* – C*i* + *1* had the exact same translation and the rotation as the motions of C*i* + *1*. For example, Fig. 2 presents the

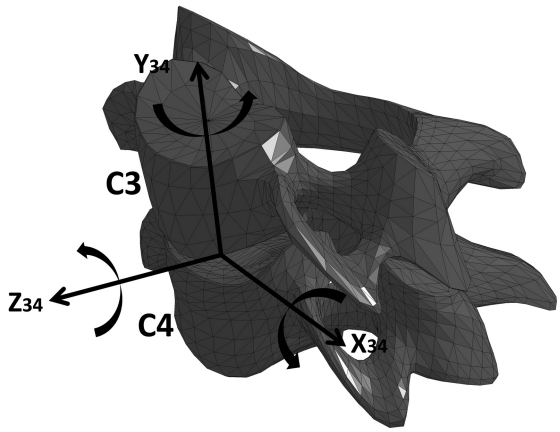

2 The C3–C4 local coordinate system.

local coordinate system of C3–C4. When the head was in the neutral position gesture, the X_{34}-, Y_{34}-, and Z_{34}-axes of the C3–C4 local coordinate system were parallel to the global coordinate axes X-, Y-, and Z-axes of the new headforms. The local coordinate system of C3–C4 was fixed on C4. The relative movements of C0–C1 to C6–C7 were defined as the relative rotations of C0–C1 to C6–C7 around their corresponding local coordinate axes.

VALIDATION OF THE NEW HEADFORM MODELS

To validate the new headform models, different quasi-static moment loads were applied on C0 (back part

of the head) as shown in Fig. 1 and LS-DYNA software (Livermore Software Technology Corporation, Livermore, CA, USA) was used to simulate the head movements. In our simulations, two constraints were implemented: nodes in the cervical vertebra C7 were set as fixed nodes that did not have translational or rotational movements during the simulations; bone layers under the forehead, left cheek, right cheek and chin segments, and the back of the head were considered as one rigid body. Table 4 gives the definitions of moment loads for the total head movements that included the extension, flexion, left rotation, and right rotation (Van der Horst, 2002).

Pure moment loads were applied to the back of the head along the X_{67}-, and Y_{67}-axes of C6–C7 local coordinate system. The pure moment loads were $M_X = 0.33$, 0.5, 1.0, 1.5, and 2.0 Nm (for the flexion), $M_X = -0.33$, −0.5, −1.0, −1.5, and −2.0 Nm (for the extension), $M_Y = 0.33$, 0.67, and 1.00 Nm (for the left rotation), and $M_Y = -0.33$, −0.67, and −1.00 Nm (for the right rotation), respectively. For example, moment load M_X was the product of the distance between the C0 mass center and the X_{67}-axis times a force applied to the C0 mass center and perpendicular to the X_{67}-axis. Once the moment load was defined, the distance and the force were automatically calculated by LS-DYNA. These values of moment loads were obtained from experiments (Panjabi *et al.*, 2001; Wheeldon *et al.*, 2006) to ensure the experimental and simulation conditions were the same in order to validate the rotation angles under the same load situation. The load curve of each pure moment began from zero, increased to the assigned moment value at the time t = 1 s, and remained the same until the end of the simulation.

During the simulation, LS-DYNA software determined the time step as 5×10^{-6} s based on convergent criteria, and the results were saved every 0.04 s. Using the medium size new headform, 16 different simulations (4 s pure moment load) were conducted. A simulation usually took ~3 s to reach a static posture. At the static posture, the velocity and the deformation rate of the headform were essentially zero. The rotation angles of C0–C1 to C6–C7 along the seven local coordinate systems were calculated at the end of each simulation and were compared with results from experiments in the literature (Panjabi *et al.*, 2001; Wheeldon *et al.*, 2006).

Table 4. Definitions of moment loads for overall head movements (Van der Horst, 2002)

Moment load (Nm)	Name
$+M_X$ = 0.33, 0.5, 1.0, 1.5, and 2.0	Flexion
$-M_X$ = −0.33, −0.5, −1.0, −1.5, and −2.0	Extension
$+M_Y$ = 0.33, 0.67, and 1.00	Left rotation
$-M_Y$ = −0.33, −0.67, and −1.00	Right rotation

RESULTS

For validating the head movements, the new medium size headform was used as one example to show the movement results with different external moments. Rotation angles for individual joints (between each pair of adjacent vertebrates) were compared. For validating the extent of flexion and extension of the new medium headform, Fig. 3 provides a comparison of rotation angles for the flexo-extension simulations for C2–C7 and reported flexo-extension experimental results (Wheeldon *et al.*, 2006). Differences in rotation angles between the simulation results and experimental results were calculated. The maximum deviations were within ±1.5°. Thus, for flexo-extension, the simulation rotation angles agreed well with the experimental rotation angles from Wheeldon *et al.* (2006).

The rotation angles of C0–C1 and C1–C2 for headform flexo-extension were also validated. Fig. 4 showed a comparison of rotation angles between the simulations and the literature (Panjabi *et al.*, 2001) for headform flexo-extension under the moments of M_X = −1.0 Nm (extension) and M_X = 1.0 Nm (flexion). The maximum difference in C0–C1 and C1–C2 joint rotation angles between the simulation results and experimental results was 2.74°, the difference of C1–C2 rotation angles in flexion.

The simulation results of the joint rotation angles in the left rotation were the same as their corresponding joint rotation angles in the left rotation. Fig. 5 shows a comparison of rotation angles between the simulations and the literature (Panjabi *et al.*, 2001) for headform rotation under the moments of M_X = 0.33, 0.67, and 1.0 Nm independently. The maximum difference appeared at the C1–C2 joint rotation angle with applied moment of M_Y = 0.33 Nm, for which the simulation result was 6.11° smaller than the experimental

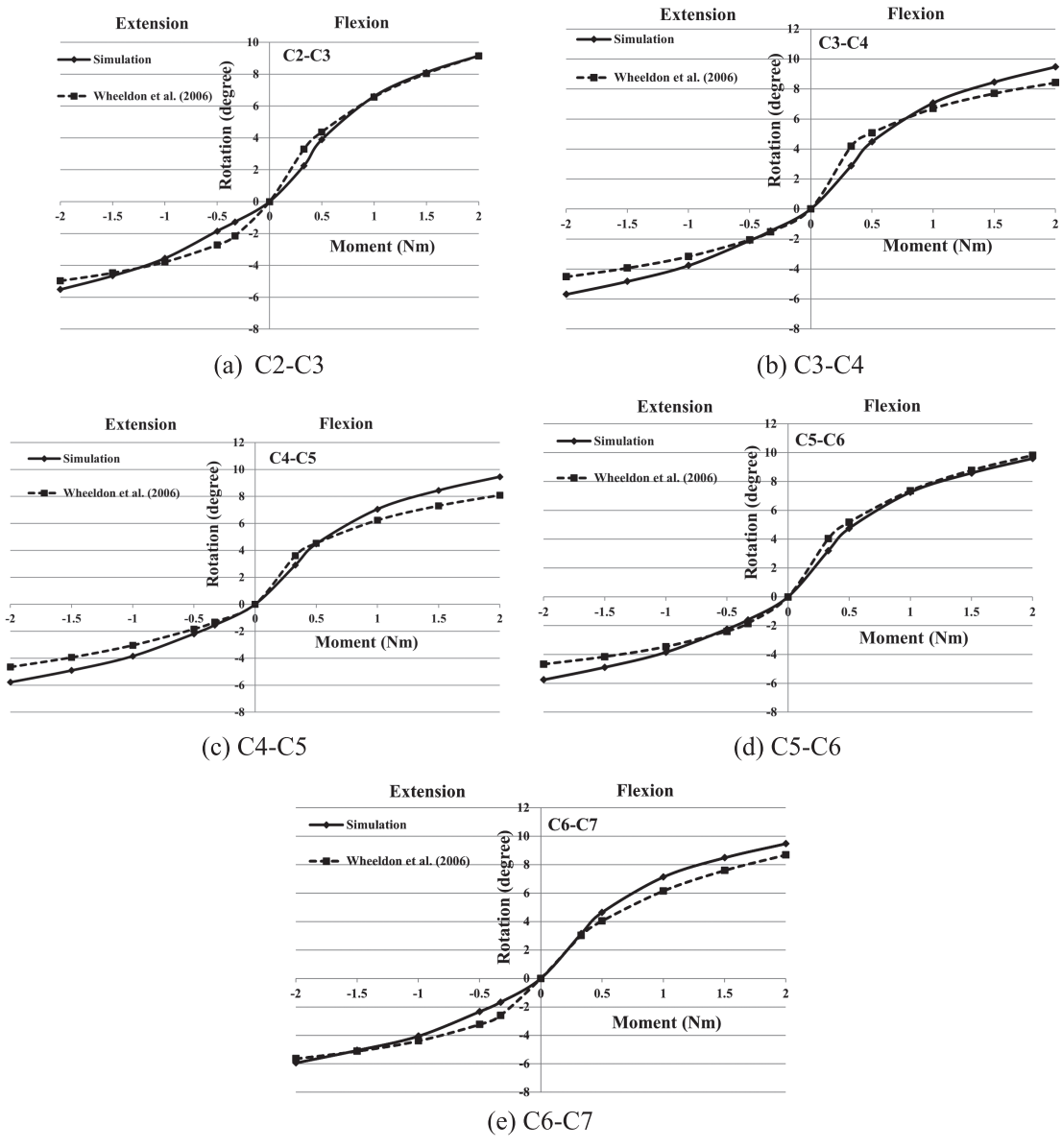

3 Comparison of rotation angles between the simulations and the literature (Wheeldon *et al.*, 2006) for headform flexo-extension under the moments of M_X = −2.0, −1.5, −1.0, −0.5, −0.33, 0.33, 0.5, 1.0, 1.5, and 2.0 Nm.

result. In the simulations with the applied moments of 1.00 Nm, the C1–C2 joint rotation angle deviations between the simulations and experiments were within ±2.6°, relatively small compared with the C1–C2 joint rotation angles (±22.4°).

DISCUSSION

The purpose of developing the motile headform models is to study the effects of head movement on contact pressure between a headform and a respirator during a respirator face seal test. The contact pressure is related to the respirator face seal characteristics. Thus, the cervical spine model in this study was simpler than that developed by del Palomar *et al.* (2008), which had deformable models as intervertebral discs, truss elements as ligaments, a contact pair as the axis and the transverse ligament, and contact pairs as facet joints. These deformable models of the intervertebral discs could

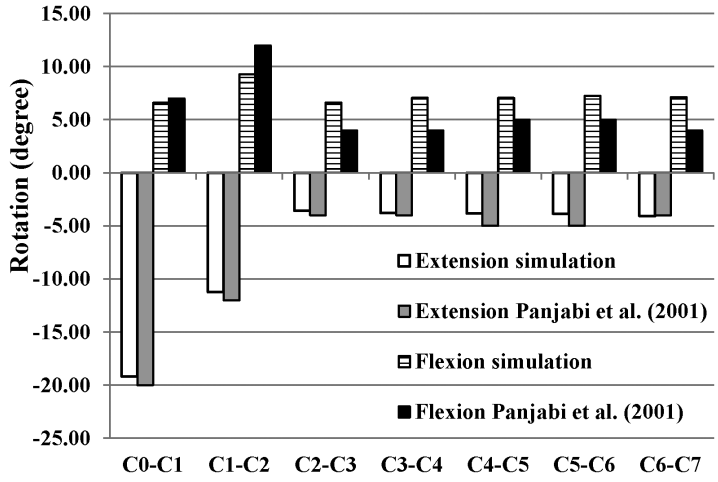

4 Comparison of rotation angles between the simulations and the literature (Panjabi *et al.*, 2001) for headform flexo-extension under the moments of M_X= −1.0 Nm (extension) and M_X=1.0 Nm (flexion).

simulate internal stresses and strains of the intervertebral discs, and the contact pairs could calculate contact pressures at the contact interfaces in the cervical spine model. However, the internal stresses and strains of the intervertebral discs and the contact pressures at the contact interfaces in the cervical spine model were not of concerns in the present study. As the dynamic calculations of deformable bodies and the surface contacts are computationally expensive, each cervical vertebra was considered as a rigid body in the cervical spine model. The authors do not expect this assumption to cause significant errors in the face seal characteristics.

In the validation for flexo-extension of individual cervical joints, the maximum deviations were within ±1.5° for C2–C7 joint rotation angles and within ±2.74° for C0–C2 joint rotation angles. Thus, for flexion and extension, the simulation rotation angles agreed well with the experimental rotation angles. For the left and right rotation, both the experimental results and simulation results had a similar pattern that the C1–C2 joints showed the highest rotation angles (~22°). The C1–C2 joint rotation angle differences between the simulations and experiments were ±6.11° (with M_Y= ±0.33 Nm moment load), ±3.09° (with M_Y= ±0.67 Nm moment load), and ±2.65° (with M_Y= ±1 Nm moment load).

There were several potential error sources. The experimental C1–C2 joint rotations in left and right rotation had a neutral zone, in which the C1–C2 joint rotation angle with M_Y= 0 Nm had an uncertain value in a range between −20° and 20°. The simulation C1–C2 joint rotation angles in left and right rotation did not have this neutral zone and always had certain values. The reason not to simulate the neutral zone was that a contact simulation between the motile headform and a respirator with head movement required certain C0–C1 to C6–C7 joint rotation angles instead of uncertain values caused by the neutral zone. The simulation C1–C2 joint rotation angles with M_Y= ±0.33 Nm were ±13.9° (31% different from their corresponding experimental joint rotation angles) and were within the value range of C1–C2 joint rotation angle from the experimental neutral zone. Although C1–C2 joint angle deviation was relatively large, the total resultant (accumulated) neck joint angles were similar between simulation and experimental results. We do not expect any significant negative effect of these errors on the study of motile headform-respirator contact.

The second error source was caused by treating the intervertebral discs as spherical joints. For more accurate results, the intervertebral discs could be modeled as FE solid models (del Palomar *et al.*, 2008). A third potential source of error was due to the multilayer headform model. Headforms were included in the head movement simulations for validation. However, the experimental samples consisted of seven cervical vertebrae and ligamentous soft tissues and did not have skin, muscle, fatty tissue, or nonvertebral bony components.

An advantage of the motile headform models was that the head movements can be simulated by

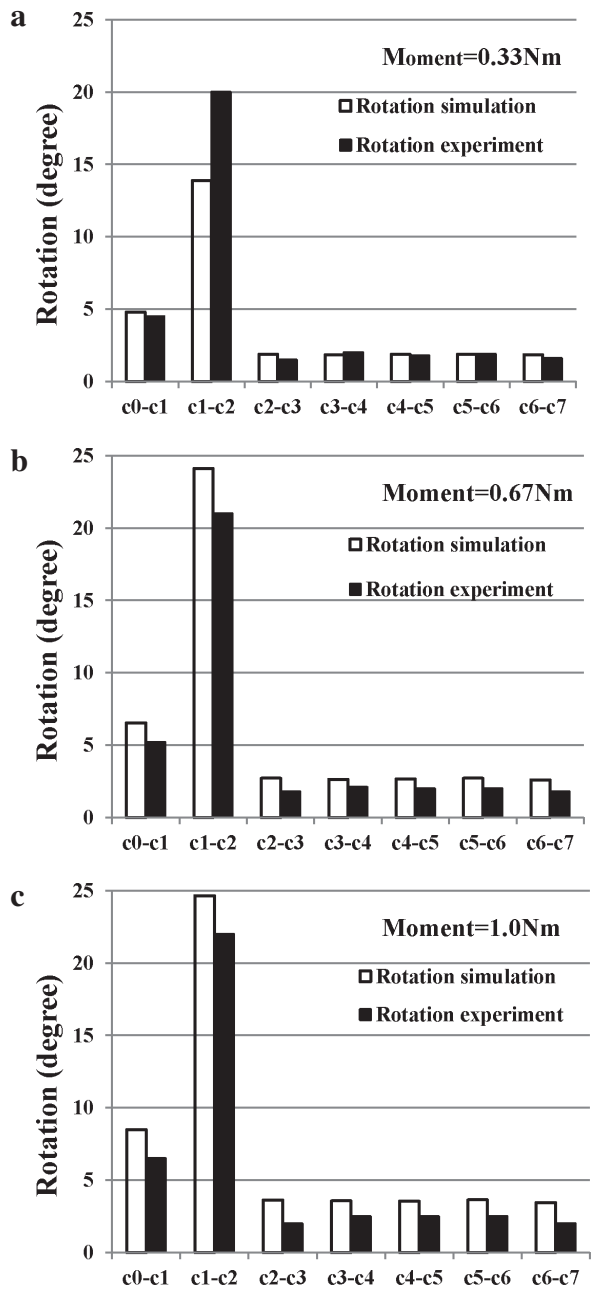

5 Comparison of rotation angles between the simulations and the literature (Panjabi *et al.*, 2001) for headform rotation under the moments: (a) $M_X = 0.33$ Nm; (b) 0.67 Nm; and (c) 1.0 Nm.

applying a single external moment load on C0 (the back of the head). The ranges of the external moment loads were 0–2 Nm for head flexo-extension and 0–1 Nm for head rotation. The final position of the head movement was the combination of C0–C7 joint rotations. In a motile headform-respirator contact simulation with head movement, the head motion can be controlled either by defining the seven joint rotation angles or by applying an external moment load. However, it is more convenient to apply an external moment load than to individually input seven joint rotation angles.

The new headform models with movement capability were developed and validated. These models will be used for respirator simulations and results will be presented in a separate paper.

FUNDING

National Institute for Occupational Safety and Health (254-2009-M-31878, 254-2010-M-36735, and 254-2012-M-52258).

ACKNOWLEDGMENTS

The authors appreciate the anonymous reviewers and editor, Lisa Brosseau, for the constructive comments and suggestions to improve the quality of this paper.

DISCLAIMER

The findings and conclusions in this paper are those of the authors and do not necessarily represent the views of the National Institute for Occupational Safety and Health.

REFERENCES

Barbarino GG, Jabareen M, Trzewik J *et al.* (2009) Development and validation of a three-dimensional finite element model of the face. *J Biomech Eng*; 131: 041006.

Beldie L, Walker B, Lu Y *et al.* (2010) Finite element modelling of maxillofacial surgery and facial expressions–a preliminary study. *Int J Med Robot*; 6: 422–30.

Bitterman BH. (1991) Application of finite element modeling and analysis to the design of positive pressure oxygen masks. Master Thesis. WrightePatterson Air Force Base, OH: Air Force Institute of Technology.

Chabanas M, Luboz V, Payan Y. (2003) Patient specific finite element model of the face soft tissues for computer-assisted maxillofacial surgery. *Med Image Anal*; 7: 131–51.

Crutchfield CD, Fairbank EO, Greenstein SL. (1999) Effect of test exercises and mask donning on measured respirator fit. *Appl Occup Environ Hyg*; 14: 827–37.

Dai J, Yang J, Zhuang Z. (2011) Sensitivity analysis of important parameters affecting contact pressure between a respirator and a headform. *Int J Ind Ergonom*; 41: 268–79.

del Palomar AP, Calvo B, Doblaré M. (2008) An accurate finite element model of the cervical spine under quasi-static loading. *J Biomech*; 41: 523–31.

Delalleau A, Josse G, Lagarde JM *et al.* (2008) A nonlinear elastic behavior to identify the mechanical parameters of human skin in vivo. *Skin Res Technol*; 14: 152–64.

Drake RL, Vogl W, Mitchell AWM. (2005) *Gray's anatomy for students*. Philadelphia, PA: Elsevier.

Engelbrektsson K. (2011) Evaluation of material models in LS-DYNA for impact simulation of white adipose tissue. Master's Thesis in Solid and Fluid Mechanics. Goteborg, Sweden: Chalmers University of Technology.

Esat V, Acar M. (2009) Viscoelastic finite element analysis of the cervical intervertebral discs in conjunction with a multi-body dynamic model of the human head and neck. *Proc Inst Mech Eng H*; 223: 249–62.

Esat V, Lopik DW, Acar M. (2005) Combined multi-body dynamic and FE models of human head and neck. *IUTAM Sympos Impact Biomech;* 124: 91–100.

Goel VK, Clausen JD. (1998) Prediction of load sharing among spinal components of a C5-C6 motion segment using the finite element approach. *Spine*; 23: 684–91.

Grinshpun SA, Haruta H, Eninger RM *et al.* (2009) Performance of an N95 filtering facepiece particulate respirator and a surgical mask during human breathing: two pathways for particle penetration. *J Occup Environ Hyg*; 6: 593–603.

Hedenstierna S, Halldin P. (2008) How does a three-dimensional continuum muscle model affect the kinematics and muscle strains of a finite element neck model compared to a discrete muscle model in rear-end, frontal, and lateral impacts. *Spine*; 33: E236–45.

Hedenstierna S, Halldin P, Siegmund GP. (2009) Neck muscle load distribution in lateral, frontal, and rear-end impacts: a three-dimensional finite element analysis. *Spine*; 34: 2626–33.

Hendriks FM, Brokken D, Van Eemeren JTWM *et al.* (2003) A numerical-experimental method to characterize the non-linear mechanical behaviour of human skin. *Skin ResTechnol*; 9: 274–83.

Lee SA, Grinshpun SA, Adhikari A *et al.* (2005) Laboratory and field evaluation of a new personal sampling system for assessing the protection provided by the N95 filtering facepiece respirators against particles. *Ann Occup Hyg*; 49: 245–57.

Lei Z, Ji X, Li N *et al.* (2014) Effect of head movement on contact pressure between respirators and headforms: part 2-simulation. *Ann Occup Hyg*.

Lei Z, Yang J, Zhuang Z. (2012) Headform and N95 filtering facepiece respirator interaction: contact pressure simulation and validation. *J Occup Environ Hyg*; 9: 46–58.

Mitsuhashi N, Fujieda K, Tamura T *et al.* (2009) BodyParts3D: 3D structure database for anatomical concepts. *Nucleic Acids Res*; 37: D782–5.

Ng HW, Teo EC, Lee VS. (2004) Statistical factorial analysis on the material property sensitivity of the mechanical responses of the C4-C6 under compression, anterior and posterior shear. *J Biomech*; 37: 771–7.

Occupational Safety and Health Administration. (1999) *Respiratory protection. OSHA technical manual (OTM)*. Section VIII, Chap. 2. https://www.osha.gov/dts/osta/otm/otm_viii/otm_viii_2.html

Panjabi MM, Crisco JJ, Vasavada A *et al.* (2001) Mechanical properties of the human cervical spine as shown by three-dimensional load-displacement curves. *Spine*; 26: 2692–700.

Piccione D, Moyer ET Jr, Cohen KS. (1997) *Model the interface between a respirator and the human face*. Aberdeen, MD: Human Engineering and Research Laboratory, Army Research Laboratory, Aberdeen Proving Ground.

Van der Horst MJ. (2002) *Human head neck response in frontal, lateral and rear end impact loading.* Eindhoven, The Netherlands: Technisch Unisersiteit Eindhoven-University of Technology.

Viscusi DJ, Bergman MS, Novak DA *et al.* (2011) Impact of three biological decontamination methods on filtering facepiece respirator fit, odor, comfort, and donning ease. *J Occup Environ Hyg*; 8: 426–36.

Wheeldon JA, Pintar FA, Knowles S *et al.* (2006) Experimental flexion/extension data corridors for validation of finite element models of the young, normal cervical spine. *J Biomech*; 39: 375–80.

Yang J, Dai J, Zhuang Z. (2009) Simulating the interaction between a respirator and a headform using LS-DYNA. *Comput Aided Des Appl*; 6: 539–51.

Yoganandan N, Kumaresan S, Pintar FA. (2001) Biomechanics of the cervical spine part 2. Cervical spine soft tissue responses and biomechanical modeling. *Clin Biomech*; 16: 1–27.

Zhang QH, Tan SH, Teo EC (2008) Finite element analysis of head–neck kinematics under simulated rear impact at different accelerations. *Proc Inst Mech Eng H*; 222: 781–90.

Zhang QH, Teo EC, Ng HW *et al.* (2006) Finite element analysis of moment-rotation relationships for human cervical spine. *J Biomech*; 39: 189–93.

Zhuang Z, Benson S, Viscusi D. (2010) Digital 3-D headforms with facial features representative of the current US workforce. *Ergonomics*; 53: 661–71.